Laser-induced graphene electrocatalyst layer for oxygen reduction reaction in proton exchange membrane fuel cells

Materials Today Advances 30 (2026) 100823

Contents lists available at ScienceDirect

Materials Today Advances

journal homepage: www.journals.elsevier.com/materials-today-advances/

Laser-induced graphene electrocatalyst layer for oxygen reduction reaction in proton exchange membrane fuel cells

Giulia Massaglia [a,b,*], Tommaso Serra [a,b], Giuseppe Ferraro [a,b], Micaela Castellino [a,b], Giacomo Spisni [a,b], Candido F. Pirri [a,b], Sergio Bocchini [a,b], Stefano Bianco [a,b], Marzia Quaglio [a,b,**]

[a] Politecnico di Torino, Department of Applied Science and Technology (DISAT), Turin, Italy
[b] Istituto Italiano di Tecnologia, Center for Sustainable Future and Technologies@Polito, Turin, Italy

ARTICLE INFO

Keywords:
Proton exchange membrane fuel cell (PEM-FC)
Laser-induced graphene (LIG)
Nitrogen and sulfur co-doping
Heteroatom-doped carbon
Oxygen reduction reaction (ORR)
Metal-free electrocatalyst

ABSTRACT

The development of cost-effective and durable electrocatalysts capable of replacing platinum in proton-exchange membrane fuel cells (PEM-FCs) remains a major barrier to large-scale implementation. Here, we present a one-step laser-assisted strategy to produce a nitrogen and sulfur co-doped laser-induced graphene (N/S-LIG) electrocatalyst layer (EL). The EL is generated by CO_2-laser processing of a multilayer assembly composed of a NaOH-treated polyacrylonitrile (PAN) nanofiber mat deposited onto a sulfonated poly(ether ether ketone) (SPEEK) membrane. Laser irradiation enables the simultaneous in situ carbonization of both polymers, yielding a graphene-like architecture featuring hierarchical porosity and intrinsic N/S co-doping. Structural and spectroscopic analyses reveal the formation of N–C_2–S and N–C–S configurations, confirming the cooperative contribution of both heteroatoms to the catalytic function. Electrochemical measurements in acidic media demonstrate an efficient four-electron oxygen reduction reaction (ORR) pathway, with an onset potential of 0.94 V versus RHE, comparable to commercial Pt/C. Under gas-diffusion electrode operation, the N/S-LIG catalyst delivers a fivefold current increase relative to S-doped LIG, highlighting the impact of dual-heteroatom incorporation. This scalable, chemical-free method offers a direct route to high-performance, metal-free ORR catalysts, supporting the advancement of practical LIG-based electrodes for next-generation fuel cells and enabling broader adoption in energy conversion technologies worldwide applications.

1. Introduction

The increasing global energy demand and the environmental impact of traditional energy resources are driving experimental research on alternative green energy sources [1–3]. Targeting the global energy transition toward a more sustainable growth require a strong transnational commitment, closely aligned to the European decarbonization goals [4–7].

In this context, hydrogen plays a key role in achieving sustainability and energy transition goals [8,9]. Not only it represents the most promising route for integrating energy from renewables into the energy system on a large scale, but as a clean, versatile and flexible energy carrier, it acquires an enabling role for initiating electrification in the transportation sector and in hard-to-abate industrial-type processes, as well as to produce so-called "solar chemicals," with a practical contribution toward decarbonization.

To date, low/medium temperature fuel cells (Proton Exchange Membrane, PEM-FCs) represent the pivotal technology for meeting the challenge of energy conversion for future clean power generation, acquiring a complementary role to that already established for batteries [10,11]. PEM-FCs are electrochemical devices that directly convert chemical energy from a fuel, represented by hydrogen, into electrical energy, minimizing emissions and environmental impact [10]. These latter considerations, coupled with the capability of PEM-FCs to operate at near ambient temperature, make such devices very attractive [10,11]. However, PEM-FCs still have a long way to go to become commercially

* Corresponding author. Politecnico di Torino, Department of Applied Science and Technology (DISAT), Corso Duca degli Abruzzi, 24, 10129, Turin, Italy.
** Corresponding author. Politecnico di Torino, Department of Applied Science and Technology (DISAT), Corso Duca degli Abruzzi, 24, 10129, Turin, Italy.
E-mail addresses: giulia.massaglia@polito.it (G. Massaglia), tommaso.serra@polito.it (T. Serra), giuseppe.ferraro@polito.it (G. Ferraro), micaela.castellino@polito.it (M. Castellino), giacomo.spisni@polito.it (G. Spisni), fabrizio.pirri@polito.it, fabrizio.pirri@iit.it (C.F. Pirri), sergio.bocchini@polito.it (S. Bocchini), stefano.bianco@polito.it (S. Bianco), marzia.quaglio@polito.it (M. Quaglio).

https://doi.org/10.1016/j.mtadv.2026.100823
Received 6 March 2026; Received in revised form 11 May 2026; Accepted 11 May 2026
Available online 19 May 2026

viable for other than niche applications. The use of the noble metal platinum as the preferred catalyst for the anode and cathode is one of the obstacles to widespread commercialization of PEMFC, due to its high cost and environmental scarcity [12].

On the cathode side of the fuel cell, the slow reaction kinetics of the oxygen reduction reaction (ORR), which leads to high voltage losses inside the fuel cell and thus low conversion efficiency [13–16], has stimulated researchers around the world to look for alternative materials that are cheaper but perform equivalently to or even better than standard Pt.

PEM-FCs also suffer from inadequate performance and durability that result mainly from oxidation of the cathode catalyst, catalyst migration, loss of active electrode surface area, membrane degradation, and corrosion of the carbon support [17–22]. In this context, to obtain an adequate performance, the synthesis, optimization and engineering of non-noble metal catalysts received great interest in accelerating the ORR [23–25].

In recent decades, enormous attention has been devoted to carbon structures doped with heteroatoms as promising catalysts for the oxygen reduction reaction in PEM fuel cells [26]. Thanks to their high electrocatalytic properties with respect to ORR, greater chemical stability, good electrical conductivity, high specific surface area and intrinsic porosity of the carbonaceous material, and low cost [18–25], it was expected that they could effectively replace the Pt/C catalyst.

Despite high expectations, particularly for nitrogen-doped carbon nanostructures, several studies in the literature have shown that nitrogen-doped carbon nanomaterials are actually effective substitutes for the Pt/C during ORR, when applied in an alkaline environment [27–30]. Indeed, due to its high electronegativity, nitrogen doping in the carbon lattice redistributes the charge density. This interaction with neighbouring carbon atoms enhances O_2 adsorption and weakens the O–O bonds, promoting a direct ORR pathway with efficient four-electron transfer [27–30]. In addition to N-doped carbon materials, other heteroatoms, such as P, S and B, act as dopants for carbon materials [27,31–38] and can play a pivotal role to improve electrocatalytic behaviour of carbon-based catalyst layers toward ORR, making them one of the most promising candidates to substitute Pt in alkaline media.

After extensive and in-depth searching, it was possible to define that one of the main constraints of these heteroatoms-doped carbon materials can be identified in their fast degradation and low ORR performance in acidic media, limiting their application as catalyst layers in acidic polymer electrolyte membrane (PEM) fuel cells [39–43]. To overcome these limitations, new strategies to tune heteroatoms doped-carbon nanomaterials were investigated with a focus on co-doping to improve catalytic performance for ORR [43–45].

Therefore, many studies investigated the importance of modulating active sites by controlling different types of doping and balancing their content, including N/S, N/P and N/S/P doped CNTs [33,34], graphene [35–39] and graphite [40–45]. Indeed, it was demonstrated how the co-doping, i.e. the doping by two different heteroatoms, was effective in inducing more active sites for the ORR than the simple increase of content of a single heteroatom [46,47]. Indeed, in co-doping the heteroatoms play a synergic effect that significantly enhances their properties [47]. Among all possible heteroatoms, the presence of N and S in the carbon structure ensured the synergic dissociation of oxygen by nitrogen and proton transfer by sulfur atoms, enhancing the electro-catalytic properties of final co-doped catalyst layers and their stability in acidic environments [48,49].

Herein, a fast, versatile, effective and new method was proposed to tune and control the incorporation of N and S heteroatoms in carbon-based nanomaterials, through the CO2 laser-induced conversion of synthetic polymeric precursors. Electrospun polyacrylonitrile nanofibers (PAN-NFs), with a high yield of carbonization and large amount of nitrogen, were directly deposited onto sulfonated poly (ether ether ketone) (SPEEK) membrane, supported carbon paper (CP), employed as electron collectors. Upon CO2 laser irradiation, both PAN-NFs and SPEEK were simultaneously transformed into Laser-Induced Graphene (LIG), resulting in a novel N/S- LIG catalyst suitable for direct oxygen reduction reaction (ORR).

Although previous studies have successfully demonstrated the conversion of SPEEK to LIG in air [50], this work proposes for the first time the direct laser-assisted conversion in air of electrospun PAN nanofibers to LIG nanofibers (LIG-NFs), according to a base-mediated process.

The obtained LIG-NFs preserve the intrinsic nanostructured features, exhibiting continuous porosity and a high surface-to-volume ratio, while featuring a self-induced nitrogen doping that generates abundant intrinsic active sites for ORR. Moreover, the simultaneous laser conversion of SPEEK introduces inherent sulfur doping, effectively addressing the common issue of catalyst instability in acidic media.

This study establishes a novel in situ dual-conversion and self-co-doping approach, where both the nitrogen and sulfur functionalities arise intrinsically from the precursor chemistry, eliminating the need for any external dopants or post-treatment steps, and yielding a robust, catalytically active LIG-based layer with outstanding ORR performance.

X-ray photoelectron Spectroscopy (XPS) analysis was carried out to confirm the achievement of successful N/S co-doping in the final LIG catalyst layer, a key feature underpinning their promising electrocatalytic activity toward ORR under acidic conditions. The electrochemical performance of the LIG-based nanocatalysts was systematically investigated using Rotating Ring-Disk Electrode (RRDE) measurements, which revealed a dominant 4-electron ORR pathway. To further validate their practical applicability in energy conversion devices, the prepared cathode catalysts were integrated into a Gas Diffusion Electrode (GDE) configuration, demonstrating their suitability for fuel cell applications.

2. Results and discussion

The rational design of heteroatom-doped carbon nanomaterials is essential for achieving efficient metal-free ORR catalysts. To overcome the limited doping versatility of conventional Polyimide (PI)-derived LIG [50–56], a dual laser-conversion strategy enabling the in-situ formation of N/S-doped LIG from synthetic polymeric precursors was implemented. Electrospun PAN nanofibers were deposited on a sulfur-rich SPEEK membrane, and CO_2-laser irradiation induced the simultaneous carbonization of both layers, yielding a self-assembled N/S-LIG architecture [57]. The novelty of this approach lies in the first demonstration that electrospun nanofibers derived from synthetic polymers can be directly transformed into LIG.

A mild NaOH/ethanol pretreatment was found essential for the successful laser conversion in ambient condition. The alkaline medium moderated the heating rate through moisture-assisted cooling and prevented excessive ablation of the nanofibers [58], while sodium ions acted as promoters for graphitic carbon formation with hierarchical porosity of the resulting catalyst [59],inducing an activation process that enhance the surface area and the defects density, both the properties being beneficial to improve the ORR performance.

The synthetic pathway leading to the formation of N/S-LIG is depicted in Scheme 1.

As confirmed by Scanning Electron Microscopy (SEM) images, the resulting material exhibits a hierarchical porous morphology distinct from standard PI-derived LIG. Raman and XPS analyses confirm the formation of graphene-like domains together with simultaneous incorporation of nitrogen and sulfur species. Notably, the direct laser conversion of PAN nanofibers, reported here for the first time, resulted in enhanced defect density and abundant catalytic sites. These structural features play a crucial role in the electrocatalytic behavior discussed in the following sections.

2.1. Morphological and chemical-physical characterizations

The CO_2 laser conversion preserves the nanostructural features of the

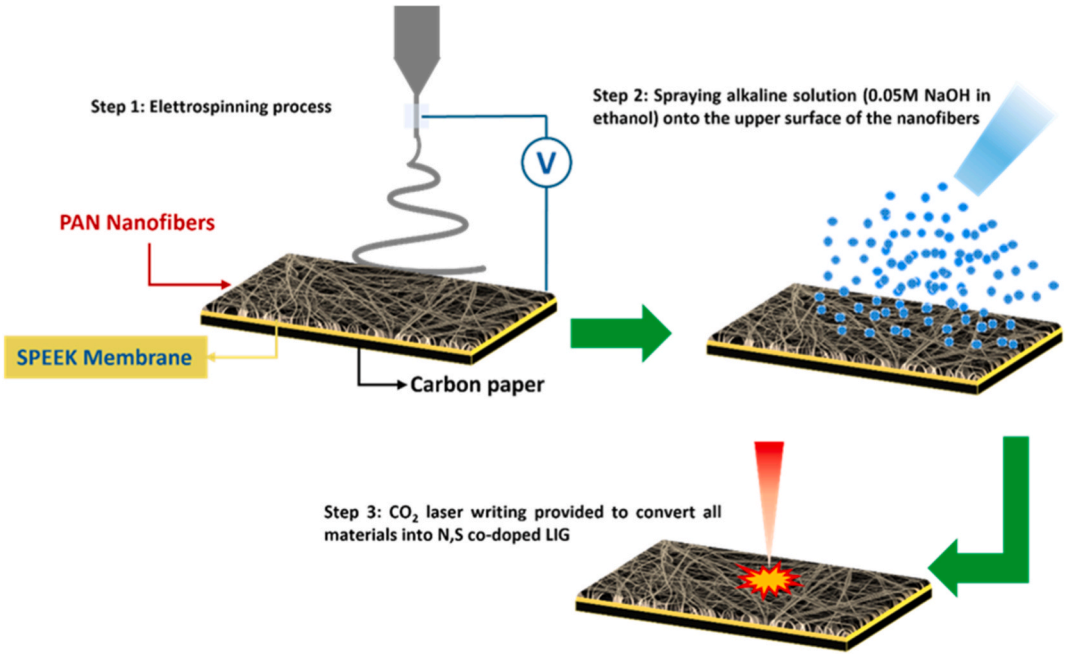

Scheme 1. Represents all steps followed to design and optimize final N, S co-doped LIG. Step 1 consist of electrospinning process implemented to ensure the deposition of PAN-based nanofibers onto SPEEK membrane; step 2 is based on spraying alkaline solution (0.05M NaOH in ethanol) onto the upper surface of nanofibers to ensure the transformation of PAN-NFs into LIG-NFs, preserving nanostructuration and step 3 reports CO2 laser process provided to ensure the simultaneous conversion of PAN-NFs and SPEEK membrane into LIG materials, defined in the present work N,S co-doped LIG.

PAN-NFs, producing LIG-nanofibers (LIG-NFs) that retain their high porosity and surface area while introducing self-generated nitrogen functionalities acting as active sites for ORR. Meanwhile, the simultaneous conversion of the underlying SPEEK membrane introduces sulfur species, ensuring co-doping without external reagents or post-treatments. This intrinsic self-co-doping mechanism, achieved through the laser processing itself, not only simplifies material synthesis but also improves the catalytic stability and activity under acidic conditions, typically a major challenge for carbon-based ORR catalysts. To validate the morphological integrity and hierarchical structure of the obtained materials, Fig. 1 provides a detailed SEM analysis of the surface architecture of the LIG samples, highlighting how the proposed laser

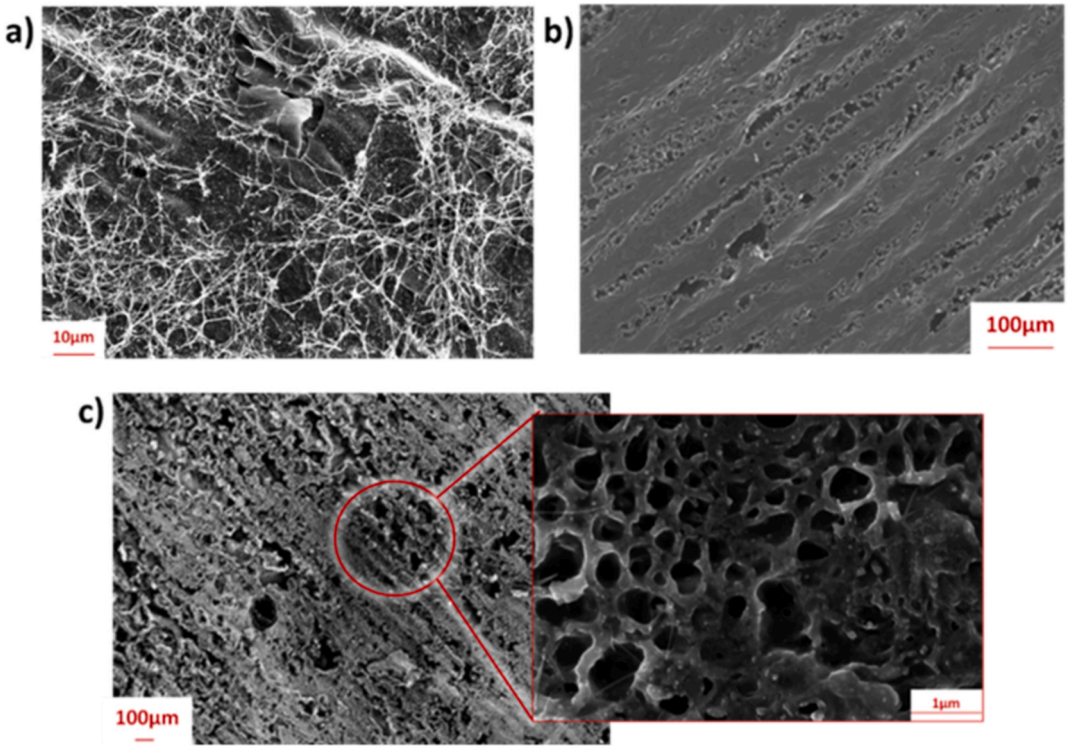

Fig. 1. SEM characterizations. Morphological properties of a) LIG-NFs with a preserved nanostructuration after CO_2 laser process; b) LIG-S obtained by transforming SPEEK membrane into LIG materials; c) N/S-LIG obtained by simultaneous in-situ conversion of PAN_NFs, SPEEK membrane.

approach effectively preserves nanostructural features while promoting porosity, key parameters to optimize ORR performance. In particular, Fig. 1a) confirmed the preservation of the nanostructures in the LIG-NFs, thus demonstrating the ability of the process proposed in the patent to ensure the transformation of PAN-NFs into LIG nanofibers, completely avoiding disruptive effects regarding the structuring. LIG-NFs maintained the intrinsic properties of nanofibers in terms of high continuous porosity and high surface area to volume ratio. Fig. 1b) reports the morphological characteristics of LIG-S, obtained by converting SPEEK membrane through CO_2 Laser writing. As described in published reference work [51], LIG-S showed a foam-like appearance combined with a porous structure distributed across different scales. It is important to note that the N/S-LIG, exhibits a greater porosity than that obtained in LIG-S samples and closer to the characteristic porosity of LIG-NFs (Fig. 1c)). This last consideration leads to the conclusion that N/S-LIG played a fundamental role in increasing the triple phase boundaries, responsible for the improvement of the electrocatalytic properties of the final catalyst layers.

The degree of graphitization for all the synthetized nanomaterials was characterized with Raman spectroscopy. The correspondent spectra are collected in Fig. 2a). LIG-S, LIG-NFs and N/S-LIG exhibit the three characteristic peaks of LIG-materials, evidencing a turbostratic arrangement [52–54]. D-peak at about 1350 cm^{-1} was representative of disordered features of graphene [52–54]. G-peak close to 1566 cm^{-1} characterized the symmetry and order of graphene; and 2D-peak at about 2688 cm^{-1} was indicative of the second-order Raman peak of double phonon resonance to reflect the stacking mode of carbon atom layers [51–54]. The higher ratio of D-band to G-band (close to 1) for N/S-LIG suggested the abundant presence of defects inside the graphene plane that can act as active catalytic sites. At the same time, by evaluating the intensity ratio between 2D-band and G-band, characteristic of graphene layers in all samples, it was determined that both N/S-LIG and LIG-S exhibited comparable I_{2D}/I_G values, close to 0.9 which lies within the range associated with few-layers graphene.

XPS spectroscopy was performed to investigate the elemental composition and doping states of N/S-LIG, with the aim of elucidating the presence of nitrogen- and sulfur-related active sites, which are known to play a crucial role in determining the electrocatalytic behaviour toward the ORR in acidic media. Considering that LIG-NFs exhibited self-induced N-doping and LIG-S showed effective S-doping (as reported in Figure S1 and Figure S2, and summarized in Table S2 and Table S3), a key objective of this study is to evaluate the capability of the CO_2 laser writing process to induce and tune the formation of N/S-LIG. The resulting material incorporates N- and S-containing functional groups that are electrochemically active toward the oxygen reduction reaction. The XPS high-resolution spectra are presented in Fig. 3, and the corresponding quantitative data are summarized in Table 1. The results clearly demonstrate the effectiveness of laser processing in introducing both N and S atoms into the final LIG structure.

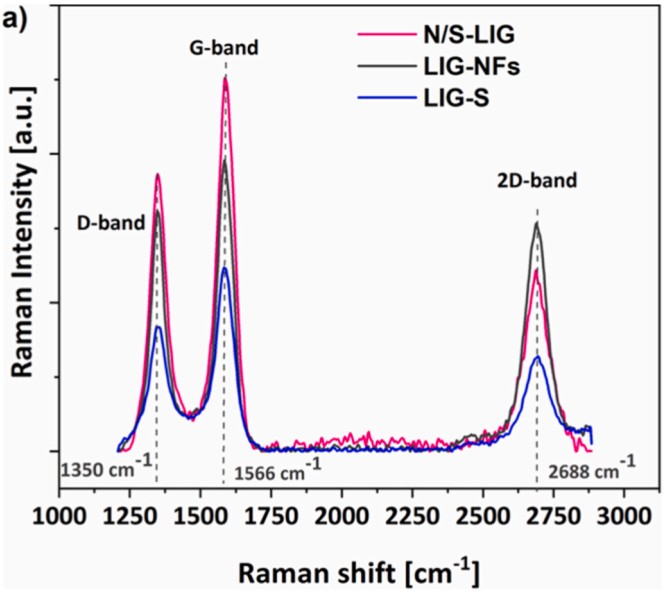

Fig. 2. a) Raman spectra of all LIG-obtained nanomaterials: i) LIG-NFs (dark grey line) obtained by implementing CO_2 laser writing onto electrospun nanofibers; ii) LIG-S (blue line) obtained by providing CO_2 laser writing onto SPEEK membrane; iii) N/S-LIG (Pink line) achieved through on an in-situ conversion/transformation at the same moment of PAN-NFs and SPEEK membrane into LIG material to design catalytic layer.

Deconvolution of the C 1s peak (see Fig. 3a)) revealed four distinct components, associated with sp^2 hybridized C–C bonds, which was fitted with an asymmetric curve (LA), which is the highest component (77.7%), meaning that the graphitization procedure was effective, while mixed Gaussian-Lorentzian (GL-30) curves have been used for fitting the curves related to C–N/S bonds (9.7%), C–O species (10.8%) and the characteristic π–π* shake-up structure (1.8%), further confirming the formation of heteroatom-doped graphitic domains [60].

To identify and quantify the individual nitrogen species within the catalyst, the high-resolution N 1s spectra were deconvoluted into their characteristic components. As shown in Fig. 3b, N/S-LIG predominantly contains pyridinic-N (≈399.5 eV) (75.1 %) and graphitic-N (≈401.4 eV) (24.9 %), two species widely recognized for enhancing the electrocatalytic activity of heteroatom-doped carbon materials toward ORR [56–59]. As discussed, co-doping with nitrogen and sulfur is expected to yield a new class of LIG materials with improved electrocatalytic performance and stability in acidic environments.

To this end, the S 2p region of the laser-treated SPEEK was also examined (see Fig. 3c). The spectra display two main features at approximately 164 and 165 eV, corresponding to the S $2p_{3/2}$ and S $2p_{1/2}$ spin–orbit components, respectively. These peaks are commonly associated with thiophenic (C–S–C) sulfur (9.7 %), typically located at edge or defect sites of the carbon lattice, and known to contribute significantly to ORR enhancement [59–74]. In N/S-LIG, two additional peaks appear at 168.3 eV and 169.5 eV, attributed to sulfonic groups (90.3 %) [50,61,62].

Thus, the high-resolution C, N and S spectra indicate the coexistence of pyridinic C–N species and neighbouring C–S bonds exhibiting partial metallic character. The close interaction between these heteroatom-doped sites is known to generate synergistic effects that govern the formation of ORR active centres [63–68]. Overall, these findings confirm the successful laser-assisted synthesis of an electrochemically active N/S-co-doped LIG material, displaying promising ORR activity for proton exchange membrane fuel cell applications [62,63].

2.2. *Electrochemical characterization in acidic media*

The electrochemical performance of the N/S-LIG was systematically assessed using a rotating ring–disk electrode (RRDE) configuration, providing insights into its catalytic behaviour under realistic operating conditions. N/S-LIG was tested in 0.1 M $HClO_4$ electrolytes and its electrocatalytic performance was continuously compared with the one achieved by LIG-S, LIG-NFs and CP, used for all of them as substrate (data reported in Supporting Information).

Cyclic voltammetry measurements under oxygen-saturated conditions (Fig. 4) revealed a more pronounced cathodic feature at ~0.5 V vs. Ag/AgCl for the N/S-LIG compared to the LIG-S (Figure s3), indicating enhanced ORR kinetics.

Subsequent analyses confirmed that the simultaneous incorporation of N and S heteroatoms significantly improved the catalytic efficiency toward the ORR. As shown in Fig. 5a), the disk current density of the N/S-LIG exceeded the ring current across the potential range, demonstrating superior ORR activity, with the corresponding onset and half-wave potentials, respectively close to 0.94V vs RHE and 0.84V vs

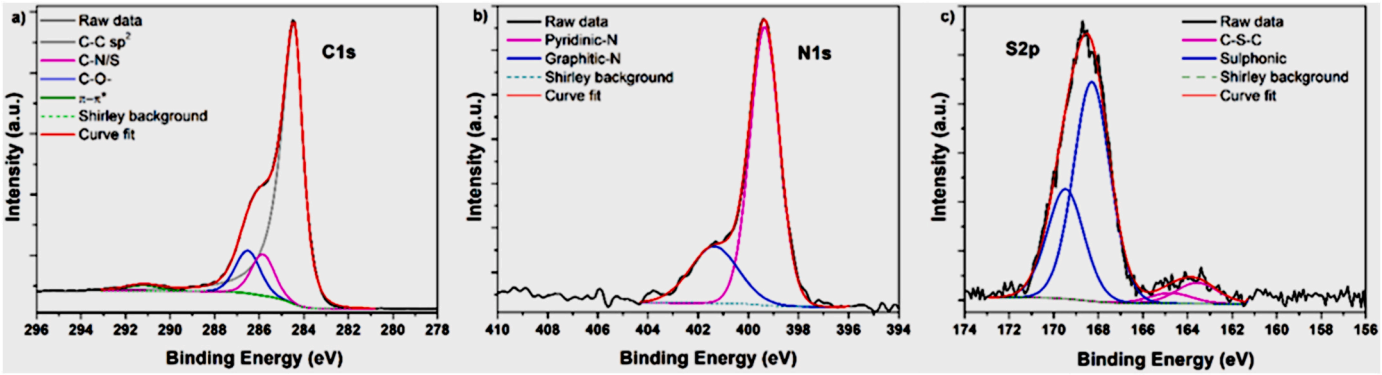

Fig. 3. XPS results obtained by analyzing N, S co-doped LIG, leading thus to define which functional groups characterized final LIG samples: a) High resolution C1s spectrum; b) N1s spectrum and c) S2p spectrum; all of them are analyzed to evaluate the presence of sulfur atoms as co-doping atom, ensured by in-situ transformation of PAN-NFs and SPEEK membrane, through the implementation of CO2 laser writing.

Table 1
XPS relative atomic concentration values (at.%) and deconvolution results from N1s and S2p regions.

Relative atomic Concentration [at.%]	
C1s	77.6
O1s	12.6
N1s	8.1
S2p	1.7
C1s peak deconvolution results [%]	
C-C sp^2	77.7
C-N/S	9.7
C-O-	10.8
p-p* shake-up	1.8
N1s peak deconvolution results [at%]	
Pyridinic-N	75.1
Graphitic-N	24.9
S2p peak deconvolution results [at%]	
C-S-C	9.7
Sulfonic group	90.3

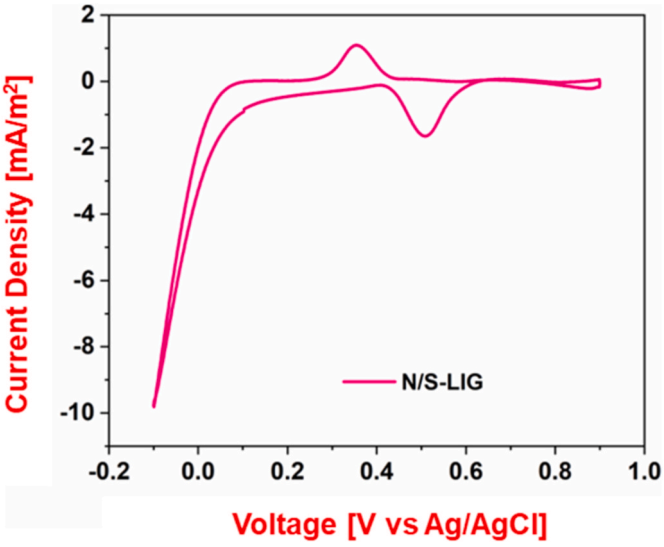

Fig. 4. Cyclic Voltammetry employed on N/S-LIG in the RRDE setup; scan rate 10 mVs^{-1}; 0.1M $HClO_4$; oxygen gas flow rate 30mLmin^{-1}.

RHE. As summarized in Table s4, it was possible to assess that the onset potential of N/S-LIG is comparable with the one achieved when 20 wt% of Pt/C is used as catalyst layer, while the half wave potential is lower than Pt/C, but outperform existing carbon materials based electrocatalysts [67–77]. All these results places N/S-LIG among the most promising heteroatom-doped carbon catalysts reported for ORR in acidic media.

The number of transferred electrons and the percentage of peroxide formation, derived from Equation (1) (described in Experimental Section) and plotted in Fig. 5b), further substantiated the enhanced catalytic pathway.

The N/S-LIG exhibited an average electron transfer number of approximately 3.91, higher than the 3.75 showed by *LIG-S* and the 3.50 achieved by *LIG-NFs,* as depicted in Figure s4. Among the materials under analysis in this work, the *LIG-NFs* showed the worst electrocatalytic behaviour in acidic media, with a dominant 2 electrons reaction path as demonstrated by a percentage of hydrogen peroxide close to the *79.9%.* This behaviour is overcome by the new N/S-LIG, that thanks to the co-doping showed an excellent electrocatalytic stability with a reduction of peroxide production close to the 5%.

These findings confirm the synergistic effect of nitrogen and sulfur co-doping in optimizing the electronic structure and active site distribution of LIG for efficient ORR catalysis. Although preliminary electrochemical indicators (low peroxide yield and near 4-electron pathway) suggest good catalytic stability, systematic long-term durability tests are currently under investigation.

2.3. *Half cell testing in gas diffusion electrode setup (HC-GDE SetUP)*

With the purpose to demonstrate that the new N/S-LIG catalyst could be successfully used as GDEs for PEM-FCs and the one-shot process here reported easily added to fabricate GDEs, we decided to test and evaluate the N/S-LIG catalyst in a half-cell gas diffusion electrode configuration (*HC*-GDE *SetUp*). Such systems [61], beyond assessing the intrinsic catalytic activity of the material, allows to appreciate the formation of a well-defined triple-phase boundary (TPB), i.e. the interfacial region where the gaseous reactants, the solid catalyst, and the liquid electrolyte simultaneously interact. The information that can be obtained by tests in the *HC-GDE SetUp* is thus more complete and of particular importance towards the use of the new materials in PEM-FC, since it offers insights in the performance of the overall active interface created during the ORR.

HC-GDE SetUps have recently gained attention as an intermediate platform bridging conventional RRDE measurements and full-cell operation, since the promising ORR performance often observed in RRDE experiments does not always translate directly under realistic working conditions [61].

The linear sweep voltammetry (LSV) profile obtained in the GDE setup (Fig. 6) exhibited a distinct ORR peak at approximately 0.6 V vs. RHE. Compared to the LIG-S tested under identical conditions, the N/S-LIG displayed a more than fivefold increase in current density, clearly demonstrating the beneficial effect of dual heteroatom doping. The

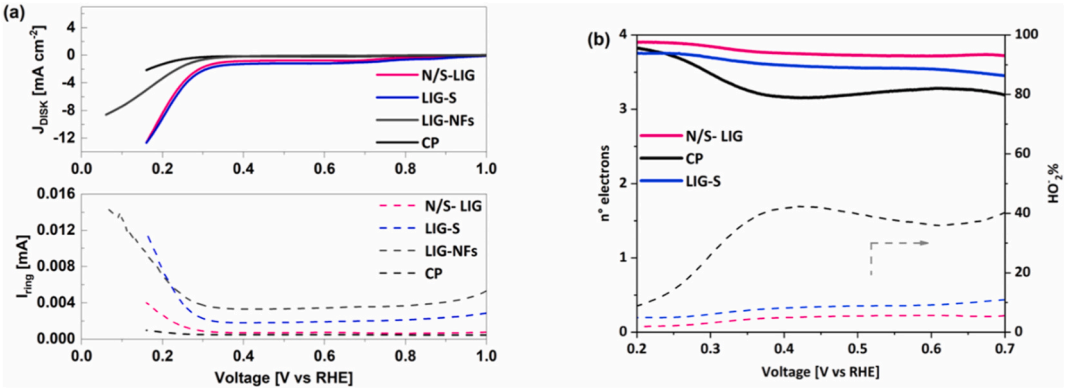

Fig. 5. (a) Current Disk and Ring density referred to N/S-LIG (pink line); LIG-S (blue line); LIG-NFs (dark grey line) and Carbon Paper, as reference material (black line); (b) number of electrons (continuous lines) and H_2O_2 production (dashed lines) to evaluate the electrocatalytic properties of all tested materials.

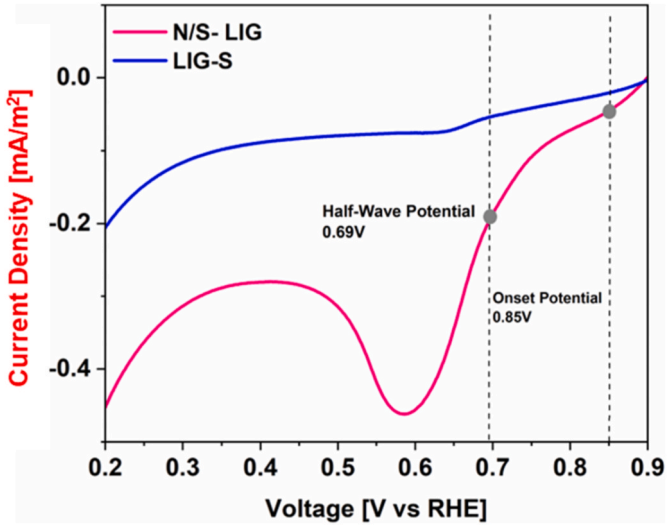

Fig. 6. Linear sweep voltammetry in HC-GDE SetUP comparing LIG-S and N/S-LIG samples.

onset and half-wave potentials were consistent with those derived from RRDE measurements, with a minor shift toward lower potentials, an expected behaviour given that the GDE setup provides a more application-relevant environment where mass transport and interfacial phenomena impose additional constraints on catalyst performance.

Beyond confirming the RRDE findings, the successful operation of the N/S-LIG catalyst in the GDE setup validated the overall functionality of the complete gas diffusion electrode, comprising the carbon paper substrate, and catalyst layer, composed by N/S-LIG, under realistic conditions. This outcome provides strong evidence that the laser-fabricated LIG-based electrodes can be effectively integrated as catalyst layers into full fuel cell assemblies, paving the way toward their practical application.

The same electrochemical characterization was carried out on LIG-NFs, which consist exclusively of catalyst layers. As shown in Fig. S6, the material exhibits a discernible electrocatalytic activity toward the ORR, attributable to the incorporation of N-heteroatoms within the nanostructured carbon matrix. Nevertheless, the recorded current density was notably limited, likely due to flooding phenomena occurring near the catalyst surface, which hindered effective gas diffusion. In addition, the catalytic layer demonstrated poor stability under acidic conditions, further constraining its overall electrochemical performance.

All achieved results allowed demonstrating for the first time the feasibility of laser assisted techniques involved in designing electroactive catalysts, simplifying the fuel cell production chain. The synergistic interaction between nitrogen and sulfur dopants in the LIG framework proved to be a key factor in enabling its excellent electrocatalytic behaviour.

3. Conclusion

The synergistic interaction between nitrogen and sulfur dopants in the LIG framework proved to be a key factor in enabling its improved electrocatalytic behaviour. In summary, a straightforward one-step LIG process was successfully developed to achieve N, S co-doping on a multilayer architecture composed of NaOH-treated PAN nanofibers and SPEEK. The resulting N, S co-doped carbon catalyst demonstrates the combined effect of nitrogen and sulfur incorporation. To the best of our knowledge, it represents the first demonstration of in situ laser-induced synthesis on a microporous layer of a catalytic layer based on graphene doped with heteroatoms.

The coexistence of N–C_2–S and N–C–S configurations within the graphene lattice was verified through XPS spectra and consistent with electrochemical results. Furthermore, both RRDE and GDE analyses confirm the synergistic contribution of the heteroatoms toward the ORR. Remarkably, the LIG technique emerged as an efficient route capable of simultaneously synthesizing and depositing carbon-based ORR catalysts in a single step. These findings demonstrate that targeted carbon doping, typically requiring multiple chemical and thermal post-treatments, can instead be accomplished directly during the laser-induced graphitization process by selecting appropriate LIG-compatible precursors.

This simplified, single-step approach offers a ready-to-use LIG catalyst featuring optimized morphology and embedded heteroatoms tailored for ORR, highlighting a significant advance toward scalable, cost-effective fabrication of functional electrodes for fuel cell applications.

4. Experimental Section

4.1. SPEEK films and nanofibers synthesis

This work developed heteroatom-doped carbon nanomaterials with tailored composition and structure is crucial to enhance the electrocatalytic performance toward the oxygen reduction reaction. In this scenario, a new dual strategy, based on the CO_2 laser process and the consequent synthesis of LIG, was proposed to synthetize the simultaneous formation of nitrogen- and sulfur-doped LIG.

In particular, the deposition of PAN nanofibers (NFs) directly onto SPEEK membrane, supported on carbon paper (Sigracet 28 BC Carbon Paper (CP) with microporous, purchased from Fuel Cell Store, USA), was achieved by implementing the electrospinning process. As deeply

investigated in our previous work [56], PAN polymer (Mw = 150 kDa, purchased from Sigma Aldrich) was selected thanks to its high yield of carbonization and a larger content of nitrogen inside its polymeric chain. Furthermore, the electrospinning process ensured the collection of PAN nanofibers mats directly on SPEEK membrane, without further materials act as binder to adhere the nanofibers' mat on the substrate.

Moreover, SPEEK membranes with diameters ranging from 5 cm to 10 cm and a thickness of just a few micrometres, were produced using a procedure similar to that described in our previous work [49,50]. Since the present work illustrated for the first time the capability to convert electrospun nanofibers derived from synthetic polymers into LIG through the implementation of CO_2 laser writing under ambient condition, it was important to describe in detail the procedure followed to synthesize all materials: *i)* LIG-NFs, that is the conversion of PAN NFs deposited onto substrate and converted into LIG; *ii)* LIG-S, which represents the conversion of SPEEK membrane into LIG materials and *iii)* N/S-LIG based on the nitrogen and sulfur heteroatoms doped LIG materials, obtained by the simultaneous conversion of PAN NFs deposited onto SPEEK membrane, supported on carbon paper. All CO2 laser writing process were summarized in Table s1. All final LIG materials were supported onto Carbon paper, as reference substrate for the functional and electrochemical characterizations.

To convert the synthetic polymers, such as PAN nanofibers, into LIG materials through CO_2 laser process in ambient condition, a pre-treatment with alkaline solution results to be mandatory. To this purpose, as electrospun PAN nanofibers were manually and carefully sprayed with a 0.05M NaOH-containing ethanol-based solution. NaOH treatment was applied to promote the controlled carbonization of PAN nanofibers. The hydroxyl groups reduced the heating rate by moisture evaporation, while sodium species facilitated graphitic carbon formation and contributed to the development of hierarchical porosity in the final N/S-LIG structures. The transformation of all materials into LIG-samples was ensured by implementing CO_2 laser writing (purchased from Laser Veronesi, nominal power of laser source equal to 10W), equipped with a pulsed CO_2 source was employed in the fabrication of LIG-containing samples. The conversion processes were all carried out under ambient conditions, applying a power of approximately 60% of maximum nominal power and a pulse frequency of 20 kHz. The beam is controlled by a galvanometric scanner, and the spot diameter is 270 μm on sample.

Both SPEEK and NFs could be converted into LIG via photothermal processing initiated by pulsed CO_2 laser radiation [50,51]. Thin NFs and SPEEK films could be converted entirely into LIG due to their low thickness, but they also became fragile in the process. For this reason, they were deposited onto a CP support that provides these materials with the necessary mechanical support.

4.2. Physico-chemical and morphological characterizations

Morphological characterizations were performed with a Zeiss Supra 40 Field Emission Scanning Electron Microscope (FESEM) to investigate the nanostructures preservation also after CO_2 laser writing and the capability to induce a hierarchical porosity distribution inside the final N, S, co-doped LIG, exploiting the intrinsic porosity of nanofibers and the active role of NaOH to modulate the porosity of carbon materials [78,79]. It is important to clarify that N, S co-doped LIG was supported onto Carbon Paper substrate for morphological investigations. To evaluate the LIG quality, characterizing all obtained materials, such as LIG-NFs, LIG-S and N, S, co-doped LIG, Raman spectroscopy studies were performed with a Renishaw inVia Reflex micro-Raman spectrophotometer with a excitation wavelength of 514.5 nm. The laser spot was ~20 μm in diameter.

X-ray Photoelectron Spectroscopy (XPS) was carried out with a PHI 5000 Versaprobe II scanning X-ray photoelectron spectrometer (monochromatic Al Kα X-ray source with 1486.6 eV energy) to investigate the surface chemical composition and chemical bonds of all LIG samples. Survey and High-Resolution (HR) spectra were acquired on spots of diameter equal to 100 μm.

4.3. Electrochemical characterizations

Electrochemical characterizations were performed with a CH1760E electrochemical workstation (CH Instruments, Inc., Bee Cave, TX, USA). An RRDE-3A Rotating Ring Disk Electrode Apparatus (ALS Co., Ltd, Tokyo, Japan) was used to characterize the intrinsic catalytic capabilities of the samples. RRDE experiments were conducted in 0.1 M perchloric acid ($HClO_4$ 70%, Sigma–Aldrich, St. Louis, Missouri, USA) electrolyte in a four-electrodes configuration to polarize both the disk and ring electrodes at the same time. A Nafion TM 117 containing solution as binder (ca. 5% in a mixture of aliphatic alcohols and water, Sigma Aldrich, St. Louis, Missouri, USA) was used to fix all LIG-based synthetized materials onto the disk-shaped Glassy Carbon working electrode. The counter electrode was based on graphite rod. The reference electrode was an Ag–AgCl electrode (197 mV versus Reference Hydrogen Electrode) (BioLogic RE-1B reference electrode, in 3 M NaCl). A rigorous comparison of the electrochemical behaviour of the two catalyst layers toward ORR requires accounting for their similar loading. Specifically, the loading of N/S LIG was set at 5.7 mg/cm^2, which is close to that of LIG/S, at approximately 7.9 mg/cm^2.

The fourth electrode was connected to the platinum ring to define the remaining content of reduced HO_2^- in the electrolyte, to derive the number of electrons involved in the ORR reaction, and to compare the disk and ring currents, as reported in Equation (1).

$$n = 4 \cdot \frac{I_D}{I_D + \frac{I_R}{N_C}}$$
$$H_2O^- = 2 \cdot \frac{\frac{I_R}{N_C}}{I_D + \frac{I_R}{N_C}} \quad (1)$$

Where I_D and I_R are respectively Disk current and Ring Current, while $N_C = 0.4$ represents RRDE collection efficiency.

In this setup, the electrolyte has been saturated with gases (Nitrogen or Oxygen) for at least 20 min prior to the measurements. With the main aim to investigate the electrocatalytic properties of all LIG-based materials, Cyclic Voltammetry characterizations were performed with the same setup in all configurations (Nitrogen-saturated and Oxygen-saturated electrolyte).

4.4. Half cell test with a gas diffusion setup

In recent years, GDE systems have established themselves as an intermediate stage between RRDE and full cell setups. They are often referred as half-cell configurations, in which the electrolyte remains in liquid form instead of solid ion-conducting polymer membrane, but, at the same time, the full electrode can be evaluated. Oxygen in its gaseous state diffuses through the porous electrode to reach active sites, and a three-phase boundary forms at the GDE–electrolyte interface between ions in the liquid electrolyte, gaseous oxygen, and solid-state catalyst [80]. GDE measurements were obtained with a Gaskatel FlexCell–PTFE electrochemical test cell.

For all these tests, an aqueous electrolyte containing 2 M perchloric acid ($HClO_4$ 70%, Sigma–Aldrich, St. Louis, Missouri, USA) was selected and a three-electrodes configuration was used. The working electrode was created by applying copper tape to the back of the samples. The purpose of this preparation technique is to optimize electrical contact among all samples, and the gold-plated banana plugs existing out of the Gaskatel Flex Cell. Counter electrode consisted of graphite rod, while the reference was Hydrogen Electrode. An exposed active area of 1 cm^2 was created, in direct contact with electrolyte, by wrapping the samples with

insulating tape.

For the half-cell tests using a gas diffusion electrode (GDE) setup, the same catalyst loading was adopted, with N/S LIG (12 mg) comparable to LIG/S (approximately 15 mg). To perform GDE measurements, N_2 and O_2 were supplied to the back side of the LIG-based electrodes at a constant flow rate of 300 mL min^{-1}. Both gases diffuse through the electrodes, reaching electrocatalytically active sites where the oxygen reduction reaction occurs.

Funding

This work received (partial) financial support from the National Recovery and Resilience Plan (NRRP) of the Italian Ministry of University and Research (Project code: IR0000027, CUP: B33C22000710006, Project title: iENTRANCE).

This work received (partial) financial support under the National Recovery and Resilience Plan (NRRP), Mission 4, Component 2, Investment 1.1, Call for tender No. 104 published on 2.2.2022 by the Italian Ministry of University and Research (MUR), funded by the European Union – NextGenerationEU– Project Title Strategy-CUP 20222H42ZP.

CRediT authorship contribution statement

Giulia Massaglia: Conceptualization, Data curation, Formal analysis, Methodology, Supervision, Validation, Writing – original draft. **Tommaso Serra:** Data curation, Formal analysis, Investigation, Writing – review & editing. **Giuseppe Ferraro:** Investigation, Methodology, Resources, Writing – review & editing. **Micaela Castellino:** Data curation, Writing – review & editing. **Giacomo Spisni:** Data curation, Writing – review & editing. **Candido F. Pirri:** Funding acquisition, Project administration, Supervision. **Sergio Bocchini:** Data curation, Visualization. **Stefano Bianco:** Data curation, Writing – review & editing. **Marzia Quaglio:** Funding acquisition, Investigation, Project administration, Supervision, Writing – review & editing.

Declaration of competing interest

The authors declare the following financial interests/personal relationships which may be considered as potential competing interests:

Giulia Massaglia has patent ##WO WO202324270 licensed to Licensed to Assigneee. Candido F. Pirri has patent ##WO WO202324270 licensed to Licensed to Assigneee. Marzia Quaglio has patent ##WO WO202324270 licensed to Licensed to Assigneee. Giulia Massaglia, Candido F. Pirri and Marzia Quaglio are inventors on a patent application (WO WO2023242701) related to the reported technology for LIG nanofibers synthesis. The authors declare no additional conflicts of interest. Moreover, I confirm that no authors of this manuscript have any competing financial or non-financial interests, currently or previously, including serving in an editorial capacity for the journal we are submitting to. If there are other authors, they declare that they have no known competing financial interests or personal relationships that could have appeared to influence the work reported in this paper. If there are other authors, they declare that they have no known competing financial interests or personal relationships that could have appeared to influence the work reported in this paper.

Appendix A. Supplementary data

Supplementary data to this article can be found online at https://doi.org/10.1016/j.mtadv.2026.100823.

Data availability

Data will be made available on request.

References

[1] K.K. Jaiswal, C.R. Chodhury, D. Yadav, R. Verma, S. Dutta, K.S. Jaiswal, B. Sangmesh, K.S.K. Karuppasamy, Renewable and sustainable clean energy development and impact on social, economic, and environmental health, Energy Nexus 7 (2022) 100118, https://doi.org/10.1016/j.nexus.2022.100118.

[2] M. Shahbaz, A. Siddiqui, M. Siddiqui, Z. Jiao, P. Kautish, Exploring the growth of sustainable energy technologies: a review, Sustain. Energy Technol. Assessments 57 (2023) 103157, https://doi.org/10.1016/j.seta.2023.103157.

[3] J. Bei, C. Wang, Renewable energy resources and sustainable development goals: evidence based on green finance, clean energy and environmentally friendly investment, Resour. Policy 80 (2023) 103194, https://doi.org/10.1016/j.resourpol.2022.103194.

[4] J. Moreno, L. Campagnolo, B. Boitier, A. Nikas, K. Koasidis, A. Gambir, M. G. Eguino, S. Perdana, D.J. Van de Ven, A. Chiodi, E. Delpiazzo, H. Doukas, M. Gargiulo, A. Herbst, K. Al-Dabbas, S. Alibas, F. Neuner, P. Le Mouel, M. Vielle, The impacts of decarbonization pathways on sustainable development goals in the European Union, Commun. Earth Environ. 5 (2024) 136, https://doi.org/10.1038/s43247-024-01309-7.

[5] Climate Action Tracker, 2100 Warming Projections [WWW Document], Climate Action Tracker, https://climateactiontracker.org/global/temperatures/, 2022. (Accessed 18 March 2023).

[6] UNEP, Emissions Gap Report 2022, UNEP, 2022. https://www.unep.org/resources/emissions-gap-report-2022.

[7] D.J. Van de Ven, S. Mittal, A. Gambhir, R.D. Lamboll, H. Doukas, S. Giarola, A. Hawkes, K. Koasidis, A.C. Koberle, H. Mcjeon, S. Perdana, G.P. Peters, J. Rogelj, I. Sognanes, M. Vielle, A. Nikas, A multimodel analysis of post-glasgow climate targets and feasibility challenges, Nat. Clim. Change 13 (2023) 570–578, https://doi.org/10.1038/s41558-023-01661-0.

[8] Z. Abdin, A. Zafaranloo, A. Rafiee, W. Merida, W. Lipinski, K.R. Khalipour, Hyderong as energy vector, Renew. Sustain. Energy Rev. 120 (2020) 109620, https://doi.org/10.1016/j.rser.2019.109620.

[9] F. Dawood, M. Anda, G.M. Shafullah, Hydrogen production for energy: an overview, Int. Journal of Hydrogen Energy 45 (2020) 3847–3869, https://doi.org/10.1016/j.ijhydene.2019.12.059.

[10] H. Wang, L. Yang, Analysis of proton exchange membranes for fuel cells based on statistical theory and data mining, iScience 27 (2024) 109360, https://doi.org/10.1016/j.isci.2024.109360.

[11] S. Ahmad, T. Nawaz, A. Ali, M.F. Orhan, A. Samreen, A.M. Kannan, An overview of proton exchange membranes for fuel cells: materials and manufacturing, Int. Journal of Hydrogen Energy 47 (2022) 19086–19131, https://doi.org/10.1016/j.ijhydene.2022.04.099.

[12] Y. Feng, N. Alonso-Vante. Non precious metal catalysts for the molecular oxygen-reduction reaction. Phys. Status Solidi 245 (20089 1792e806 https://doi.org/10.1002/pssb.200879537.

[13] A.M. Gomez-Marin, J.M. Feliu, Oxygen reduction on platinum single crystal electrodes, Encyclopedia of Interfacial Chemistry (2018), https://doi.org/10.1016/j.coelec.2018.03.018. Elsevier.

[14] C. Hu, L. Dai, Carbon-based metal-free catalysts for electrocatalysis beyond the ORR, Angew. Chem. Int. Ed. 55 (39) (2016), https://doi.org/10.1002/anie.201509982, 11736e11758.

[15] A. Kulkarni, S. Siahrostami, A. Patel, J.K. Nørskov, Understanding catalytic activity trends in the oxygen reduction reaction, Chem. Rev. 118 (5) (2018), https://doi.org/10.1021/acs.chemrev.7b00488, 2302e2312.

[16] J. Zhang, L. Dai, Heteroatom-doped graphitic carbon catalysts for efficient electrocatalysis of oxygen reduction reaction, ACS Catal. 5 (12) (2015), https://doi.org/10.1021/acscatal.5b01563, 7244e7253.

[17] R. Bashyam, P. Zelenay, A class of non-precious metal composite catalysts for fuel cells, Nature 443 (2006) 63e6, https://doi.org/10.1038/nature05118.

[18] K. Gong, F. Du, Z. Xia, M. Durstock, L. Dai, Nitrogen-doped carbon nanotube Arrays with high electrocatalytic activity for oxygen reduction, Science 323 (2009), https://doi.org/10.1016/j.jtice.2026.106715, 760e764.

[19] J.-C. Li, P.-X. Hou, L. Zhang, C. Liu, H.-M. Cheng, Growth of metal-catalyst-free nitrogen-doped metallic single-wall carbon nanotubes, Nanoscale 6 (2014), https://doi.org/10.1039/C4NR03172E, 12065e12070.

[20] S. Chen, J. Bi, Y. Zhao, L. Yang, C. Zhang, Y. Ma, Q. Wu, X. Wang, Z. Hu, Nitrogen doped carbon nanocages as efficient metal-free electrocatalysts for oxygen reduction reaction, Adv. Mater. 24 (2012), https://doi.org/10.1002/adma.201202424, 5593e5597.

[21] J. Liang, X. Du, C. Gibson, X.W. Du, S.Z. Qiao, N-doped graphene natively grown on hierarchical ordered porous carbon for enhanced oxygen reduction, Adv. Mater. 25 (2013), https://doi.org/10.1002/adma.201302569, 6226e6231.

[22] J.-C. Li, P.-X. Hou, S.-Y. Zhao, C. Liu, D.-M. Tang, M. Cheng, F. Zhang, H.-M. Cheng, A 3D bi-functional porous N-doped carbon microtube sponge electrocatalyst for oxygen reduction and oxygen evolution reactions, Energy Environ. Sci. 9 (2016), https://doi.org/10.1039/C6EE02169G, 3079e3084.

[23] C. Hu, L. Dai, Carbon-based metal-free catalysts for electrocatalysis beyond the ORR, Angew. Chem. Int. Ed. 55 (2016), https://doi.org/10.1002/anie.201509982, 11736e11758.

[24] A. Kulkarni, S. Siahrostami, A. Patel, J.K. Nørskov, Emerging carbon-based catalysts for the oxygen reduction reaction: insights into mechanisms and applications, iinorganics 12 (2024) 303, https://doi.org/10.3390/inorganics12120303.

[25] J.C. Li, P.X. Hou, C. Liu, Heteroatom-doped carbon nanotube and graphene-based electrocatalysts for oxygen reduction reaction, Small 13 (2017) 1702002, https://doi.org/10.1002/smll.201702002.

[26] K. Mamtani, U.S. Ozkan, Heteroatom-doped carbon nanostructures as oxygen reduction reaction catalysts in acidic media: an overview, Catal. Lett. 145 (2015) 436–450, https://doi.org/10.1007/s10562-014-1434-y.
[27] C. Yang, H. Jin, C. Cui, J. Wang, K. Amine, J. Lu, S. Wang, Nitrogen and sulfur co-doped porous carbon sheets for energy storage and pH-universal oxygen reduction reaction, Nano Energy 54 (2018), https://doi.org/10.1016/j.nanoen.2018.10.005, 1952-199.
[28] Y. Okamoto, First-principles molecular dynamics simulation of O2 reduction on nitrogen-doped carbon, Appl. Surf. Sci. 256 (2009) 335–341, https://doi.org/10.1016/j.apsusc.2009.08.027.
[29] R.A. Sidik, A.B. Anderson, N.P. Subramanian, S.P. Kumaraguru, B.N. Popov, O2 reduction on graphite and nitrogen-doped graphite: experiment and theory, J. Phys. Chem. B 110 (2006) 1787–1793, https://doi.org/10.1021/jp055150g.
[30] L. Zhang, Z. Xia, Mechanisms of oxygen reduction reaction on nitrogen-doped graphene for fuel cells, J. Phys. Chem. C 115 (2011) 11170–11176, https://doi.org/10.1021/jp201991j.
[31] J. Zhu, G. He, L. Liang, Q. Wan, P.K. Shen, Direct anchoring of platinum nanoparticles on nitrogen and phosphorus-dual-doped carbon nanotube arrays for oxygen reduction reaction, Electrochim. Acta 158 (2015) 374–382, https://doi.org/10.1016/j.electacta.2015.01.173.
[32] H. An, R. Zhang, Z. Li, L. Zhou, M. Shao, M. Wei, Highly efficient metal-free electrocatalysts toward oxygen reduction derived from carbon nanotubes @polypyrrole core-shell hybrids, J. Mater. Chem. A 4 (2016) 18008–18014, https://doi.org/10.1039/C6TA08892A.
[33] S. Zhao, J. Liu, C. Li, W. Ji, M. Yang, H. Huang, Y. Liu, Z. Kang, Tunable- ternary (N, P, B)-doped porous nanocarbon and their catalytic properties for oxygen reduction reaction, ACS Appl. Mater. Interfaces 6 (2014) 2229722304, https://doi.org/10.1021/am506284k.
[34] D. Yu, Y. Xue, L. Dai, Vertically aligned carbon nanotube arrays Co-doped with phosphorus and nitrogen as efficient metal-free electrocatalysts for oxygen reduction, J. Phys. Chem. Lett. 3 (2012) 2863–2870, https://doi.org/10.1021/jz3011833.
[35] C. Choi, M. Chung, H. Kwon, S. Park, S. Woo, B,N- and P,N-doped graphene as highly active catalysts for oxygen reduction reactions in acidic media, J. Mater. Chem. A 1 (2013) 3694–3699, https://doi.org/10.1039/C3TA01648J.
[36] S. Dou, A. Shen, Z. Ma, J. Wu, L. Tao, S. Wang, N-, P- and S-tridoped graphene as metal-free electrocatalyst for oxygen reduction reaction, J. Electroanal. Chem. 753 (2015) 21–27, https://doi.org/10.1016/j.jelechem.2015.05.013.
[37] M.D. Bhatt, G. Lee, J.S. Lee, Oxygen reduction reaction mechanisms on Al-doped X-graphene (X = N, P and S) catalysts in acidic medium: a comparative DFT study, J. Phys. Chem. C 120 (2016) 26435–26441, https://doi.org/10.1021/acs.jpcc.6b09674.
[38] F. Razmjooei, K.P. Singh, M.Y. Song, J.S. Yu, Enhanced electrocatalytic activity due to additional phosphorous doping in nitrogen and sulfur-doped graphene: a comprehensive study, Carbon 78 (2014) 257–267, https://doi.org/10.1016/j.carbon.2014.07.002.
[39] A.Z. Yazdi, E.P.L. Roberts, U. Sundararaj, Nitrogen/sulfur co-doped helical graphene nanoribbons for efficient oxygen reduction in alkaline and acidic electrolytes, Carbon 100 (2016) 99–108, https://doi.org/10.1016/j.carbon.2015.12.096.
[40] M. Sahoo, S. Ramaprabhu, Nitrogen and sulfur co-doped porous carbon – is an efficient electrocatalyst as platinum or a hoax for oxygen reduction reaction in acidic environment PEM fuel cell, Energy 119 (2017) 1075–1083, https://doi.org/10.1016/j.energy.2016.11.066.
[41] J. Shui, M. Wang, D. Feng, L. Dai, N-doped carbon nanomaterials are durable catalysts for oxygen reduction reaction in acidic fuel cells, Sci. Adv. 1 (2015) E1400129, https://doi.org/10.1126/sciadv.1400129.
[42] C.V. Pham, M. Klingele, B. Britton, K.R. Vuyyuru, T. Unmüssig, S. Holdcroft, A. Fischer, S. Thiele, Tridoped reduced graphene oxide as a metal-free catalyst for oxygen reduction reaction demonstrated in acidic and alkaline polymer electrolyte fuel cells, Adv. Sustain. Syst. 1 (2017) 1600038, https://doi.org/10.1002/adsu.201770051DigitalObjectIdentifier.
[43] B. Liu, J. Li, B. Yan, Q. Wei, X. Wen, H. Xie, H. He, P.K. Shen, Z.Q. Tian, Sulfur doped iron-nitrogen-hard carbon nanosheets as efficient and robust noble metal-free catalysts for oxygen reduction reaction in PEMFC, J. Energy Chem. 89 (2024) 422–433, https://doi.org/10.1016/j.jechem.2023.10.046.
[44] M.M. Mohideen, Q. Wang, S. Ramakrishna, Y. Liu, Chitosan-derived carbon sphere with self-activating behavior for stable oxygen reduction reaction in acid and alkaline media, Carbon 226 (2024) 119154, https://doi.org/10.1016/j.carbon.2024.119154.
[45] I. Palm, E. Kibena-Poldsepp, M. Mooste, J. Kozlova, M. Kaarik, A. Kikas, A. Treshchalov, J. Leis, V. Kisand, A. Tamm, S. Holdcroft, K. Tammevesk, Nitrogen and sulfur co-doped carbon-based composites as electrocatalysts for the anion-exchange membrane fuel cell cathode, Int. J. Hydrogen Energy 55 (2024) 805–814, https://doi.org/10.1016/j.ijhydene.2023.11.185.
[46] V. Mazanek, S. Matejkova, D. Sedmidubsky, M. Pumera, Z. Sofe, One-step synthesis of B/N Co-doped graphene as highly efficient electrocatalyst for the oxygen reduction reaction: synergistic effect of impurities, Chem. Eur J. 24 (2018) 928–936, https://doi.org/10.1002/chem.201704515.
[47] R. Sibul, E. Kibena-Poldsepp, U. Maeorg, M- Merisalu, A. Kikas, V. Kisand, A. Treshchalov, V. Sammelselg, K. Tammeveskia, Sulfur and nitrogen co-doped graphene-based electrocatalysts for oxygenreduction reaction in alkaline medium, Electrochem. Commun. 109 (2019) 106603, https://doi.org/10.1016/j.elecom.2019.106603.
[48] M. Sahoo, S. Ramaprabhu, Nitrogen and sulfur co-doped porous carbon e is an efficient electrocatalyst as platinum or a hoax for oxygen reduction reaction in acidic environment PEM fuel cell? Energy 119 (2017) https://doi.org/10.1016/j.energy.2016.11.066, 1075e1083.
[49] S.-A. Wohlgemuth, R.J. White, M.-G. Willinger, M.-M. Titirici, M. Antonietti, A onepot hydrothermal synthesis of sulfur and nitrogen doped carbon aerogels with enhanced electrocatalytic activity in the oxygen reduction reaction, Green Chem. 14 (2012) 9, https://doi.org/10.1039/C2GC35309A, 1515e23.
[50] A. Lamberti, M. Serrapede, G. Ferraro, M. Fontana, F. Perrucci, S. Bianco, A. Chiolerio, S. Bocchini, All-SPEEK flexible supercapacitor exploiting laser-induced graphenization, 2D Mater. 4 (2017) 035012, https://doi.org/10.1088/2053-1583/aa790e.
[51] T. Serra, G. Massaglia, P. Zaccagnini, M. Fontana, C.F. Pirri, G. Cicero, S. Bianco, M. Quaglio, Laser-induced graphene as electrode material in proton-exchange membrane fuel cells, Mater. Process. 14 (2023) 33, https://doi.org/10.3390/IOCN2023-14520.
[52] R. Murray, M. Burke, D. Iacopino, A.J. Quinn, Design of experiments and optimization of laser-induced graphene, ACS Omega 6 (2021) 16736–16743, https://doi.org/10.1021/acsomega.1c00309.
[53] Y. Steksova, A.C. Bressi, M. Galliani, A. Marino, G. Ciofani, E. Machado-Charry, H. G. Bernal, A. Francini, L. Sebastiani, F. Greco, Laser-induced graphene from waste almond shells, Adv. Funct. Mater. (2025), https://doi.org/10.1002/adfm.202507462.
[54] L.X. Duy, Z. Peng, Y. Li, J. Zhang, Y. Ji, J.M. Tour, Laser-induced graphene fibers, Carbon 126 (2018) 472–479, https://doi.org/10.1016/j.carbon.2017.10.036.
[55] M. Liu, J. Wu, H.Y. Cheng, Effects of laser processing parameters on properties of laser induced graphene by irradiating CO2 laser on polyimide, Sci China Tech Sci 65 (2022) 41–52, https://doi.org/10.1007/s11431-021-1918-8.
[56] G. Massaglia, M. Quaglio, A review on laser-induced graphene-based electrocatalysts for the oxygen reduction reaction in electrochemical energy storage and conversion, Nanomaterials 15 (2025) 1070, https://doi.org/10.3390/nano15141070.
[57] G. Massaglia, V. Margaria, A. Sacco, M. Castellino, A. Chiodoni, F.C. Pirri, M. Quaglio, N-doped carbon nanofibers as catalyst layer at cathode in single chamber microbial fuel cells, IJHE 44 (2019) 4442–4449, https://doi.org/10.1016/j.ijhydene.2018.10.008.
[58] S. Lee, S. Jeon, Laser-induced graphitization of cellulose nanofiber substrates under ambient conditions, ACS Sustain. Chem. Eng. 7 (2019) 2270–2275, https://doi.org/10.1021/acssuschemeng.8b04955.
[59] H. Liu, Y. Xie, J. Liu, K.S. Moon, L. Lu, Z. Lin, W. Yuan, C. Shen, X. Zang, L. Lin, Y. Tang, C.P. Wong, Laser induced and KOH-activated 3D graphene: a flexible activated electrode fabricated via direct laser writing fron in-plane micro supercapacitors, Chem. Eng. J. 393 (2020) 124672, https://doi.org/10.1016/j.cej.2020.124672.
[60] N. Garino, A. Sacco, A. Chiodoni, Candido F. Pirri, M. Castellino, Microwave-assisted synthesis of nitrogen and sulphur doped graphene decorated with antimony oxide: an effective catalyst for oxygen reduction reaction, Materials 15 (2022) 10, https://doi.org/10.3390/ma15010010.
[61] R. Ojeda-Lopez, G. Ramos-Sanchez, J.M. Esparza-Schulz, L. Lartundo, A. Dominguez-Ortiz, On site formation of N doped carbon nanofibers, an efficient electrocatalyst for fuel cell applications, Int. J. Hydrogen Energy 42 (2017), https://doi.org/10.1016/j.ijhydene.2017.08.096, 30339e48.
[62] L. Dong, W. Wang, J. Zang, Y. Zang, Z. Wang, J. Su, et al., Fe, N codoped porous carbon nanosheets for efficient oxygen reduction reaction in alkaline and acidic media, Int. J. Hydrogen Energy 43 (2018), https://doi.org/10.1016/j.ijhydene.2018.05.140, 14273e80.
[63] V. Gridin, J. Du, S. Haller, P. Theis, K. Hofmann, G.K.H. Wiberg, U.I. Kramm, M. Arenz, GDE vs RDE: impact of operation conditions on intrinsic catalytic parameters of FeNC catalyst for the oxygen reduction reaction, Electrochim. Acta 444 (2023), https://doi.org/10.1016/j.electacta.2023.142012.
[64] Vracar, L.J. Oxygen reduction reaction in acid solution. In Enciclopedia of Applied Electrochemistry; Kreysa, G., Ota, Ki, Savinell, R.F. Eds.; Springer, New York, NY. https://doi.org/10.1007/978-1-4419-6996-5_481.
[65] Guixuan Ma, Guoqing Ning, Qiang Wei, S-doped carbon materials: synthesis, properties and applications, Carbon 195 (2022) 328–340, https://doi.org/10.1016/j.carbon.2022.03.043.
[66] Yingna Chang, Jiawei Li, Tian Zhang, Jindi Wang, Danni Wang, Yu Liu, Miaosen Yang, Rong Xing, Guoxin Zhang, Correlating oxygen reduction activity of N,S-co-doped carbon with the structures of dopant molecules, J. Alloys Compd. 986 (2024) 174165.
[67] S. Nösberger, J. Du, J. Quinson, E. Berner, A. Zana, G.K.H. Wiberg, M. Arenz, The gas diffusion electrode setup as a testing platform for evaluating fuel cell catalysts: a comparative RDE-GDE study, Electrochem. Sci. Adv. 3 (2022), https://doi.org/10.1002/elsa.202100190.
[68] K. Ehelebe, N. Schmitt, G. Sievers, A.W. Jensen, A. Hrnjić, P.C. Jiménez, P. Kaiser, M. Geuß, Y.P. Ku, P. Jovanovič, K.J.J. Mayrhofer, B. Etzold, N. Hodnik, M. Escudero–Escribano, M. Arenz, S. Cherevko, Benchmarking fuel cell electrocatalysts using gas diffusion electrodes: inter–Lab comparison and best practices, ACS Energy Lett. 7 (2022), https://doi.org/10.1021/acsenergylett.1c02659.
[69] J. Liu, Yi-Gang Ji, Bin Qiao, Fengqi Zhao, Hongxu Gao, Pei Chen, Zhongwei An, Xinbing Chen, Yu Chen, N,S Co-Doped carbon nanofibers derived from bacterial Cellulose/Poly(Methylene blue) hybrids: efficient electrocatalyst for oxygen reduction reaction, MDPI Catalysts 8 (2018) 269, https://doi.org/10.3390/catal8070269.
[70] KaterynaArtyushkova SadiaKabir, andPlamenAtanassov AlexeySerov, Role of nitrogen moieties in N-Doped 3D-Graphene nanosheets for oxygen

electroreduction in acidic and alkaline media, ACS Appl. Mater. Interfaces 10 (2018) 11623–11632, https://doi.org/10.1021/acsami.7b18651.
[71] Bingqiu Liu, Qi Zhang, Z. Wang, L. Li, Z. Jin, C. Wang, L. Zhang, L. Chen, Z. Su, Nitrogen and sulfur-codoped porous carbon nanospheres with hierarchical micromesoporous structures and an ultralarge pore volume for high-performance supercapacitors, Adv. Mater. Interfac. 12 (2020) 8225–8232, https://doi.org/10.1021/acsami.9b20473.
[72] Y. Wang, S. Liu, Y. Cui, W. Bai, S. Liu, Q. Ye, F. Zhou, W. Liu, In-situ pyrolysis synthesis of multi-element (F, N, S) co-doped porous carbon nanospheres as lubricating additives with improved tribological behaviors, Carbon 218 (2024) 118724, https://doi.org/10.1016/j.carbon.2023.118724.
[73] W. Zhang, X. Guo, C. Li, J.Y. Xue, W.Y. Xu, Z. Niu, H. Gu, C. Redshaw, J.P. Lang, Ultralong nitrogen/sulfur Co-doped carbon nano-hollow-sphere chains with encapsulated cobalt nanoparticles for highly efficient oxygen electrocatalysis, Carbon Energy 5 (2023) e317, https://doi.org/10.1002/cey2.317.
[74] Kai Qin, Xiaoqiang Li, Shao Tong, Yu Zhang, Guangdi Zhang, Haimei Liu, Yongyao Xia One-step facile fabrication of N, S co-doped carbon modified NiS/MoS2 heterostructure microspheres with improved sodium storage performance, J. Power Sources 529 (2022) 231282, https://doi.org/10.1016/j.jpowsour.2022.231282.
[75] Liya Ma, Liu Jin, Lv Song, Qin Zhou, Xinyu Shen, Shaobo Mo, Hua Tong, Scalable one-step synthesis of N,S co-doped graphene-enhanced hierarchical porous carbon foam for high-performance solid-state supercapacitors, J. Mater. Chem. A 7 (2019) 7591–7760, https://doi.org/10.1039/C9TA00038K.
[76] A. Xintong, Li J. Wang, X. Duan, Y. Li, X. FanGuoliang, Z. Fengbao, Z.W. Peng, Fine-tuning radical/nonradical pathways on graphene by porous engineering and doping strategies, ACS Appl. Mater. Interfaces 11 (2021) 4848–4861, https://doi.org/10.1021/acscatal.0c05089.
[77] Y. Guo, R. Zhang, H. Hong, Y. Zhao, Z. Huang, C. Han, H. Li, C. Zhi, Ultrahigh oxygen-doped carbon quantum dots for highly efficient H2O2 production via two-electron electrochemical oxygen reduction, Energy Environ. Sci. 15 (2022) 4167–4174.
[78] A. Linares-Solano, M.A. Lillo-Ródenas, J.P. Marco-Lozar, M. Kunowsky, A. J. Romero-Anaya, NaOH and KOH for preparing activated carbons used in energy and environmental applications, Int. J. Energy Environ. Econ. 20 (2012) 59–91.
[79] G. Qin, Y. Liu, J.C. He, N. Wang, J. Wang, X. Jian, Porous hollow carbon alkali-activated nanoonions as a conductive additive for high-rate lithium primary batteries, ACS Appl. Energy Mater. 7 (2024) 7936–7944, https://doi.org/10.1021/acsaem.4c01531.
[80] R. Sharma, R. Maurya, S.M. Andersen, True gas phase oxygen reduction reaction (ORR) explorations at the electrolyte/gas interface: a unique screening configuration to study electrode interface structure for PEMFCs, J. Power Sources 641 (2025) 236841, https://doi.org/10.1016/j.jpowsour.2025.236841.